

BiFeO₃ as Electrode Material for Lithium Batteries

Luo Shihai¹, Gao Mei², Chen Jun³, Xing Xianran³, Li Zhong², Zhou Xingtai² and Wen Wen^{2,*}

¹Shanghai Institute of Applied Physics, Chinese Academy of Sciences, 2019 Baojia Road, Shanghai 201800, P. R. China

²Shanghai Synchrotron Radiation Facility, Shanghai Institute of Applied Physics, Pudong New area, Shanghai 201204, P. R. China

³Department of Physical Chemistry, University of Science and Technology of Beijing,
30 Xueyuan Road, Haidian District, Beijing, 100083, P. R.China

Received: November 15, 2010, Accepted: February 14, 2011, Available online: April 19, 2011

Abstract: BiFeO₃ was studied as electrode material for lithium battery applications. The voltage profile of BiFeO₃ vs Li battery displays three discharge plateaus around 1.3, 0.7 and 0.4 V (vs Li/Li⁺) and the first discharge capacity is about 1000 mAh/g, with a cutoff voltage of 0.05 V. If the cutoff voltage is limited to 0.7 V, much better capacity retention is achieved. The structural changes of BiFeO₃ during electrochemical cycling process were investigated using synchrotron-based *in situ* XRD and XANES. Lithium ions were inserted into BiFeO₃ during the discharge process. The whiteline of Bi L_{III}-edge XANES spectra gradually decreased during the discharge process with their L_{III} edge position concomitantly shifted towards lower energy position. However, the Fe K-edge XANES spectrum of the fully discharged product is similar to that of the pristine one and displays no shifts. This indicates that Bi ions are responsible for charge transfer during the electrochemical cycling process. The reduction of Bi³⁺ to Bi⁰ as the gradual insertion of Li ions, is a three-step reduction process. Li₂Bi alloy formation was observed at the end of the discharge process, which is not fully reversible towards lithium intercalation/extraction and decomposes to metallic Bi.

Keywords: Lithium batteries; *in situ* XRD; *in situ* XANES

1. INTRODUCTION

Lithium batteries are of great interests recently, partly due to the continuous consumption of fossil fuel and the necessary decrease of CO₂ release, which is a critical factor for global warming. In the past, various electrode materials have been investigated as potential ones for lithium ion battery applications. However, to explore new materials for energy storage is very important, especially for those having potential to be used in electric vehicles.

While in most of the studied cathodes, such as spinel, olivine and layer structure, cationic redox couple are mainly responsible for the charge transfer, the effect of O²⁻ anions, can not be neglected[1-3]. Perovskite type oxides, are thus of great interests due to its well-known high oxygen mobility, and have wide applications as electrolyte[4], fast ion conductor[5] as well as superconductor[6]. In the literature, LaFeO₃[7], CaSnO₃[8], Gd_{1/3}TaO₃[9], Li_yLa_{(1-y)/3}NbO₃[10], SrVO_{3-δ}[11], and LaCoO₃[12], etc. have been

investigated for lithium battery applications. Normally the discharge voltages of the perovskite type oxides are below 1.2 V, which are much lower compared with those of the other structures, such as spinel, olivine and layer compounds. To better understand the effect of O²⁻ during the charge transfer process, structural investigations are very necessary, while this is less explored.

Recently, BiFeO₃ polycrystalline thin film, synthesized by pulsed laser deposition method, was used as electrode material for battery application[13] and the discharge mechanism was proposed, mainly based on electrochemical cycling results. In this work, powdered BiFeO₃ was synthesized using a molten salt method, and further was used as electrode material for lithium battery application. The structural transformations occurred during the electrochemical cycling process were investigated using the synchrotron *in situ* XRD and XANES, by which not only the phase transitions can be observed in the real time but also much better signal to noise ratio can be obtained due to its high flux.

*To whom correspondence should be addressed: Email: wenwen@sinap.ac.cn
Phone/Fax.: 0086-21-33933215

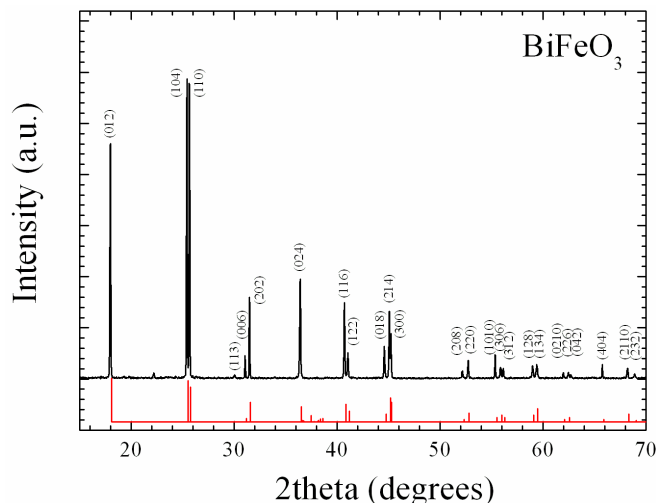


Figure 1. The XRD pattern of synthesized BiFeO_3 taken at BL14B1 of SSRF at a wavelength of 0.12398 nm, the standard diffraction pattern of BiFeO_3 is also displayed in red[15]. (JCPDS card 20-169)

2. MATERIAL SYNTHESIS AND DATA ACQUISITION METHOD

BiFeO_3 was synthesized using a molten salt route. Typically, Bi_2O_3 , Fe_2O_3 , NaCl , Na_2SO_4 , and NP-9 (nonylphenyl ether) were mixed in a molar ratio of 1:1:5:5:3, grounded for 20 minutes, and then sonicated for 10 minutes. The mixture was transferred to a crucible, pretreated at 400°C for 2 hours, and then loaded into a furnace, where the temperature was maintained at 800°C for 20 minutes before quenching to room temperature in air. Pure BiFeO_3 product was obtained after washing the quenched material several times with deionized water to remove the NaCl and Na_2SO_4 salts[14].

The electrochemical galvanostatic cycling is carried out at a current density of 20 mA/g. Typically, BiFeO_3 , PVDF (Polyvinylidene Fluoride) and acetylene black were mixed in the weight percentage of 75%, 12.5%, 12.5% in NMP (N-methyl-2-pyrrolidone) and then coated on a 0.01 mm Cu foil to make the electrode. The counter electrode is metallic lithium. For the *in situ* work, the middle of the Cu foil was cut a hole (2 mm \times 2 mm) before the electrode material was painted on, and the hole is filled with the material. The electrode is further heated in the vacuum oven at 120°C to evaporate the NMP.

The *in situ* X-ray diffraction (XRD) experiments were carried out at BL14B1 beamline of the Shanghai Synchrotron Radiation Facility (SSRF) at a wavelength of 0.12398 nm. BL14B1 is a bending magnet beamline and the storage ring energy of SSRF is 3.5 GeV. The beam is first collimated using a Rh/Si mirror and then is monochromatized using a Si(1 1 1) double crystal monochromator. After that, the beam is further focused by a Rh/Si mirror to the size of 0.5 mm \times 0.5 mm. Higher order harmonics are also rejected by the Rh/Si mirror to 3×10^{-4} . A NaI scintillation detector was used for data collection. The XRD data (ASCII format) were transformed into GSAS format and were analyzed using the CMPR

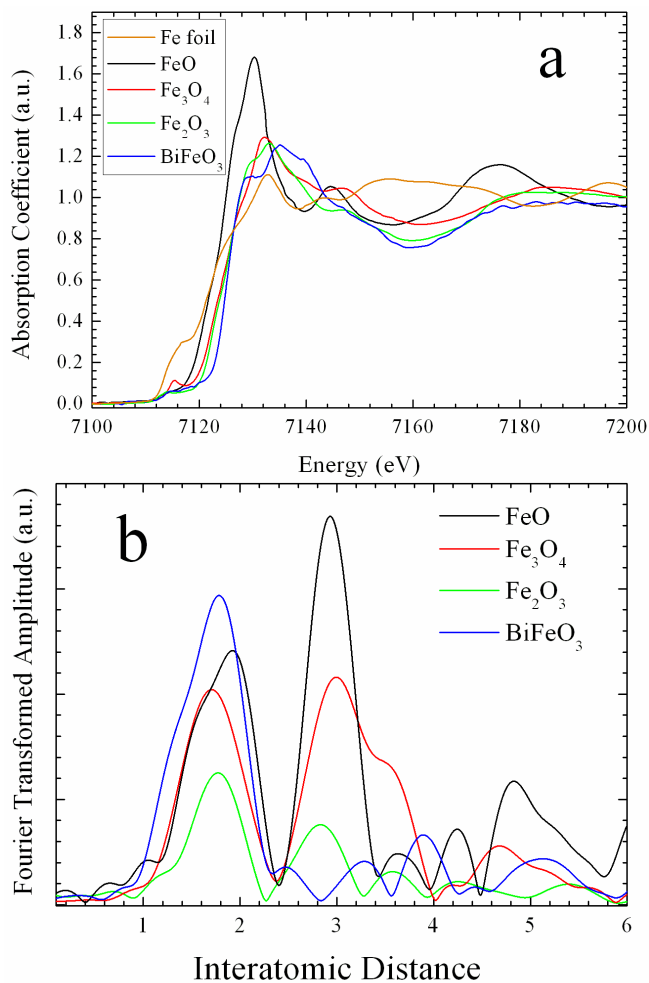


Figure 2. a) The Fe K-edge XANES spectra of 1) Orange, Fe foil; 2) Black, FeO; 3) Red, Fe_3O_4 ; 4) Green, Fe_2O_3 ; 5) Blue, BiFeO_3 . b) The Fe K-edge Fourier transformed EXAFS spectra of 1) Black, FeO; 2) Red, Fe_3O_4 ; 4) Green, Fe_2O_3 ; 5) Blue, BiFeO_3 .

program[15].

The *in situ* X-ray absorption experiments were carried out at BL14W1, which is a wiggler based beamline, of the Shanghai Synchrotron Radiation Facility (SSRF) using transmission mode. Si(1 1 1) double crystal monochromator cooled by liquid N_2 was employed to monochromatize the energy. The XANES data were analyzed by Athena code of the IFEFFIT program for background removal, E_0 selection, normalization and Fourier transformations, etc[16].

The *in situ* experiments were carried out using a spectro-electrochemical cell[17-19], which has been discussed in detail elsewhere. It is a sandwich type cell feature, which has Mylar windows in both the cathodic and anodic sides, respectively. This allows the X-ray to penetrate through the active material while it is cycled. The *in situ* cell is air-tight and thus any structural transformations observed are not because of decomposition or oxidation of the material upon air exposure.

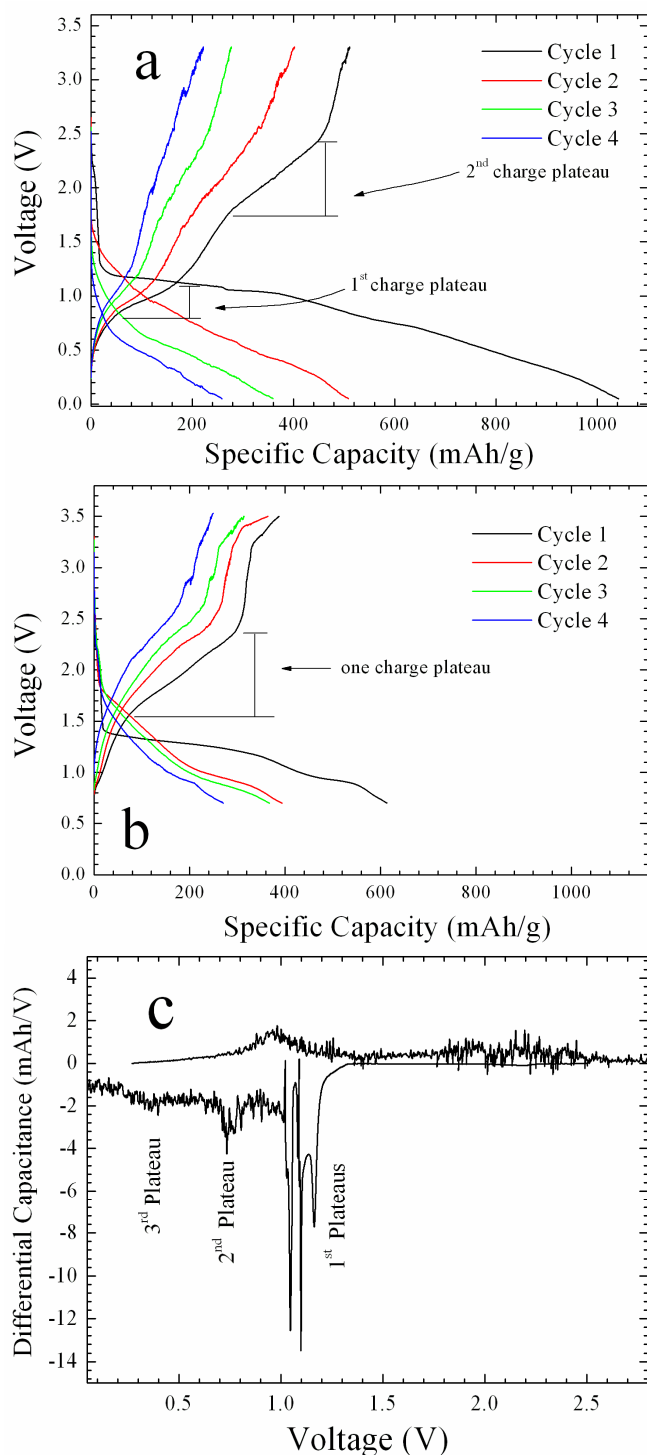


Figure 3. The galvanostatic cycling profiles of BiFeO₃ vs Li batteries, a) With the voltage window between 0.05 V ~ 3.3 V, Black) cycle 1; Red) cycle 2; Green) cycle 3; Blue) cycle 4; b) With the voltage window between 0.7 V ~ 3.5 V, Black) cycle 1; Red) cycle 2; Green) cycle 3; Blue) cycle 4; c) The differential capacitance vs voltage plot of BiFeO₃ vs Li battery using a cut off voltage of 0.05 ~ 3.3V.

3. RESULTS AND DISCUSSION

The XRD pattern of synthesized BiFeO₃ is displayed in Figure 1. It has very high crystallinity and has the space group of *R3c* (Rhombohedral, Hexagonal setting) with lattice parameters of $a = 0.5587$ nm, $b = 0.5587$ nm and $c = 1.3889$ nm. The diffraction pattern of standard BiFeO₃[20] is also displayed in Figure 1 for comparison.

The Fe k-edge X-ray absorption near edge structure (XANES) spectra of BiFeO₃, Fe₂O₃ and some standard materials are displayed in Figure 2a. The pre-edge peaks (around 7112 eV) of the FeO, α -Fe₂O₃ and BiFeO₃ are quite weak compared to that of the Fe₃O₄, where 1/3 of the Fe ions occupied the tetrahedral site positions[21]. This indicates that in FeO, Fe₂O₃ and BiFeO₃, Fe ions occupied the octahedral site positions and the coordination environments are quite symmetric. The Fe K-edge Fourier-transformed EXAFS of BiFeO₃ and some standard materials are displayed in Figure 2b. All these Fe oxides show a peak around 1.8 Å, which is the Fe-O interaction in the first coordination shell. FeO has the longest Fe-O bond distance, due to its lowest oxidation state of the Fe ions among these four oxides. Normally, in Fe oxides, the Fe-Fe interactions could be connected by corner, lattice or face, depending on the orientations of two adjacent octahedrons[22]. The Fe-Fe distance connected via corner is around 3.5 Å, and is longer than those connected via lattice or face, which are between 3.0 to 3.5 Å[22]. The latter (Fe-Fe connected via lattice/face) can be clearly observed in the Fe K-edge Fourier-transformed EXAFS spectra of FeO, Fe₂O₃ and Fe₃O₄. For perovskite BiFeO₃, the closest Fe ions can only be connected via the vertex of two adjacent octahedrons. Thus, there are no such peaks around 3.0 ~ 3.5 Å, compared to those of the other oxides.

The electrochemical cycling profiles of the BiFeO₃ vs Li battery were studied using two voltage ranges. One is using the cutoff voltage of 0.7 V and the other 0.05 V. It is observed that the 1st cycle discharge capacity is about 1000 mAh/g with a cutoff voltage of 0.05 V (Figure 3a). The voltage drops quickly to about 1.3 V and reach the first discharge plateau with a capacity about 500 mAh/g. At about 0.9 V, the 2nd discharge plateau appears and continues to the point where the discharge capacity reaches about 700 mAh/g. According to literature[10], this plateau corresponds to lithium insertion into acetylene black. Around 0.6 V, the 3rd discharge plateau appears and continues to the point where the discharge capacity reaches about 1000 mAh/g. After 0.4 V, the voltage decreases quickly to 0.05 V.

In the charge cycle, the voltage increases slowly to 0.7 V and reaches the 1st charge plateau until it finished at 1.18 V with a capacity about 200 mAh/g. This could be correlated to the 3rd discharge plateau in the discharge process. The 2nd charge plateau is located between 1.75 V to 2.5 V, which is much higher compared to the corresponding discharge plateau, indicating large polarization, mostly due to the large resistance increase after the 1st discharge process. For the 2nd cycle, the capacity in the 1.3 V region (1st plateau) is greatly decreased, if compared with the 1st cycle. This suggests that the 1.3 V plateau capacity is originated from BiFeO₃, which is partially transformed to some other structure in the 1st discharge process. In the 3rd cycle, the capacity in the 1.3 V region is further decreased, which is consistent with the previous discussion and may indicate rather sudden decay of the BiFeO₃.

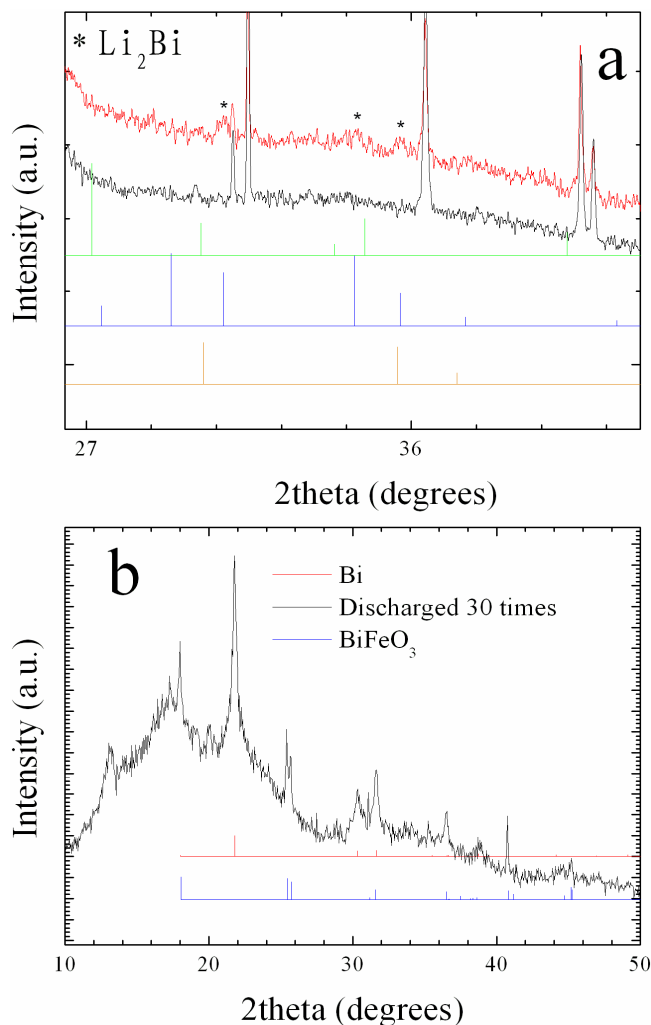


Figure 4. a) The comparison of, Black) the XRD pattern of starting material at open circuit potential; Red) the XRD pattern at the fully discharged stage; Green) the XRD pattern of LiBi ;²⁰ (JCPDS card 27-422) Blue) the XRD pattern of Li_2Bi ;²¹ (JCPDS card 45-956) Orange) the XRD pattern of Li_3Bi ;²² (JCPDS card 27-427) b) XRD patterns of, Black) The discharged material of BiFeO_3 vs Li battery after 30 times cycling with the voltage window between 0.05 ~ 3.5 V; Red) Bi ;²³ (JCPDS card 44-1246) Blue) BiFeO_3 .¹⁹ (JCPDF card 20-169).

structure. The resistance increase of the lithiated electrode might also contribute to the capacity decrease.

Figure 3b is the discharge profile of the BiFeO_3 vs Li battery with a cutoff voltage of 0.7 V, right before the appearance of the third plateau. It can be seen much clearly that there is a charge plateau located between 1.5 ~ 2.5 V, exactly corresponding to the discharge plateau around 1.3 V region. In the consequent cycles, these two correlated charge and discharge plateaus were observed with good capacity retention, suggesting a lithium insertion mechanism. However, the resistance of the lithiated BiFeO_3 might be much larger compared with the pristine BiFeO_3 and contribute to

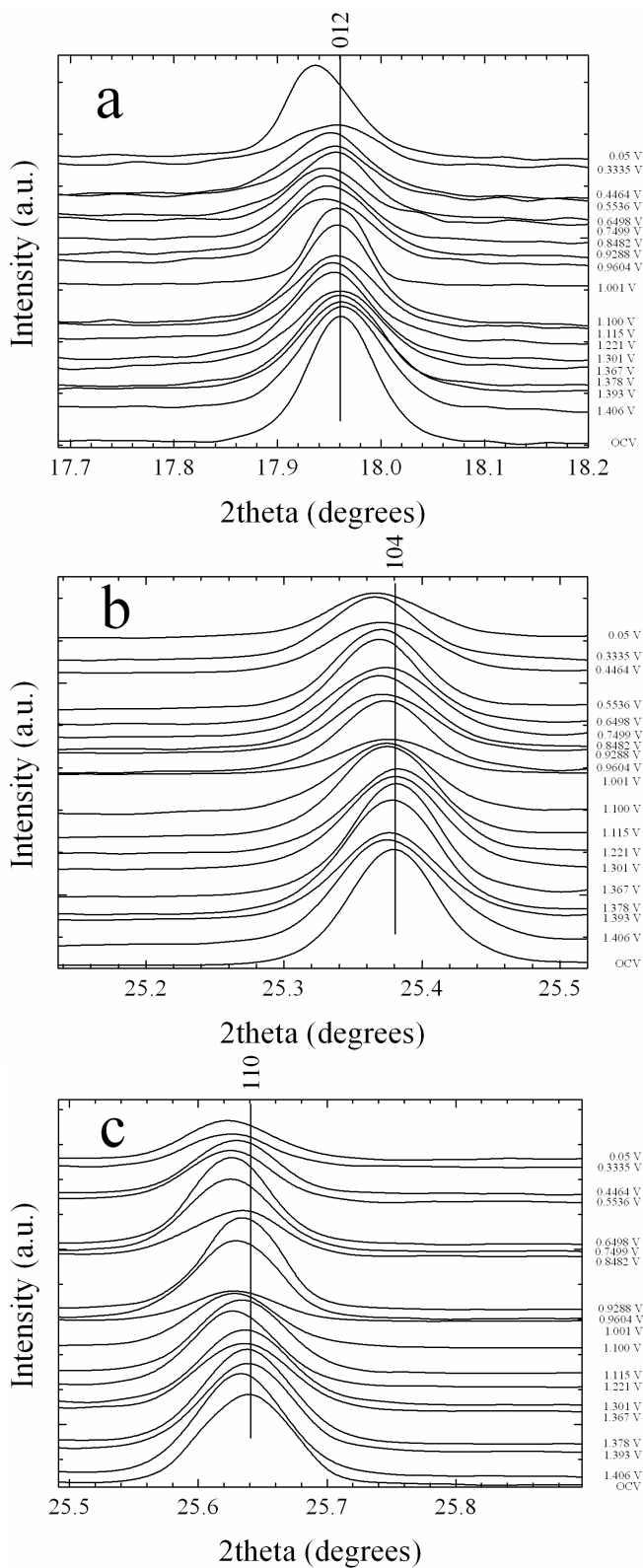


Figure 5. *In situ* XRD patterns collected during the 1st discharge process using the spectro-electrochemical cell feature, a) diffraction peak of 012; b) diffraction peak of 104; c) diffraction peaks of 110.

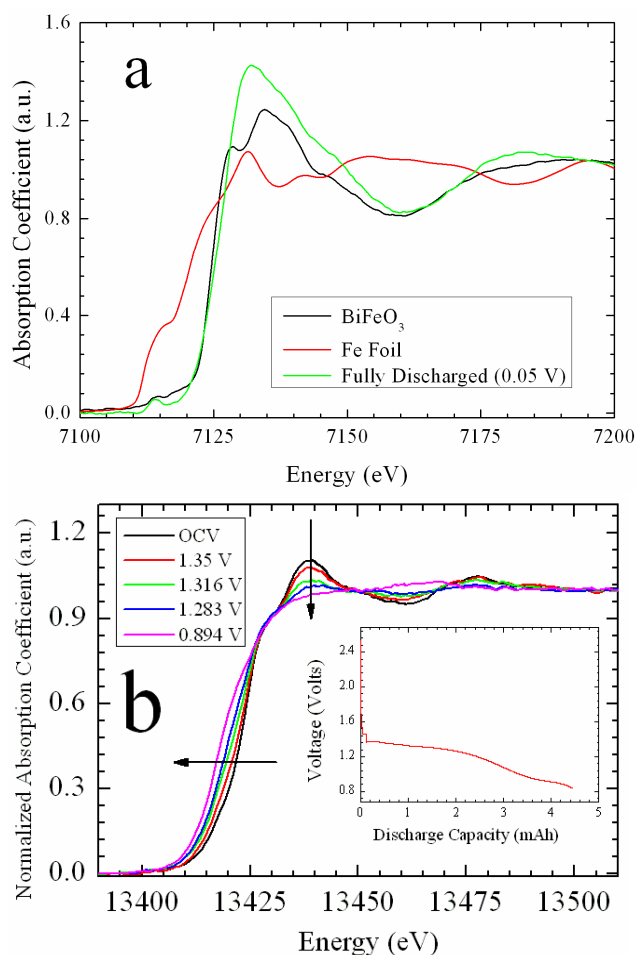


Figure 6. a) Fe K-edge XANES spectra of, Red) Fe foil; Black) BiFeO₃; Green) Fully discharged to 0.05 V; b) *In situ* Bi L_{III}-edge XANES spectra collected during the discharge process using the spectro-electrochemical cell feature, Black) Open circuit potential; Red) 1.350 V; Green) 1.316 V; Blue) 1.283 V; Pink) 0.894 V.

large polarization during the subsequent cycling process. Compared the discharge profiles of BiFeO₃ vs Li battery using these two cut-off voltages, it is obvious that when the batteries are discharged to 0.7 V, much capacity retention can be achieved. It can also be observed that when the BiFeO₃ vs Li battery is discharged using a cut-off voltage of 0.7 V, there is only one charge plateau existed in the charge process.

The differential capacitance vs voltage plot of the BiFeO₃ vs Li battery discharged between 0.05 V to 3.3 V is displayed in Figure 3c. In the 1st discharge cycle, three discharge peaks can be observed at 1.16 V, 1.10 V and 1.05 V, indicating three-step electron transfer occurred at the 1st plateau region. The 2nd discharge plateau is located around 0.75 V, corresponding to the lithium insertion into acetylene black. The 3rd discharge plateau is located around 0.36 V.

To investigate the structural changes of BiFeO₃ during the electrochemical cycling process, *in situ* XRD patterns of BiFeO₃ vs Li battery were recorded. As displayed in Figure 4a, a new structure is formed at the end of the discharge process and was assigned to

Li₂Bi[24](JCPDS card 45-956). Thus, the two plateaus during the 1st charge process highlighted in Figure 3a, corresponding to Li⁺ extraction from lithiated BiFeO₃ (1.75 V~ 2.5 V) and Li₂Bi, respectively. When the cutoff voltage is limited to 0.7 V, Li₂Bi formation is greatly suppressed and this contribute to a better capacity retention in the subsequent cycles. However, no metallic Fe and Bi diffraction peaks were observed, which might indicate a different discharge mechanism compared to that of BiFeO₃ thin film batteries, where metallic Fe and Bi was proposed to appear before the alloying process. Also using the *in situ* spectro-electrochemical cell, the BiFeO₃ vs Li battery was cycled for 30 times. The XRD pattern of the discharged material was obtained and displayed in Figure 4b. The discharged material is consisted of two major phases, lithiated BiFeO₃ and metallic Bi[26]. This indicates that Li₂Bi alloy is not fully reversible towards lithium intercalation/extraction and decomposes to metallic Bi.

Series of *in situ* diffraction patterns during the discharge process are displayed in Figures 5a, 5b and 5c. At the discharge process, it is observed that the diffraction peak 012 displays shifts, which indicates that the discharge process is a solid solution type of lithium insertion process and is consistent with the electrochemical cycling results. However, this peak is not shifted towards one single direction during the entire discharge process. Normally, the unit cell of a crystal lattice is expected to expand when Li ions are inserted into the crystal lattice.¹⁷ In BiFeO₃ case, the lithiated BiFeO₃ is not stable and LiBi tend to separate out from the crystal lattice in the form of Li₂Bi. The combination of the lithium insertion and the Li₂Bi alloy formation processes, might contribute to the diffraction peak shift observed in the 012 peak. Similar shifts are also observed in the diffraction peaks of 104 and 110.

The Fe K-edge XANES spectra of the fully discharged product were displayed in Figure 6a. The Fe K-edge XANES spectra of the fully discharged product is similar to that of the pristine one and displays no shift. This indicates that Fe ions are not reduced during the discharge process. The series of *in situ* Bi L_{III}-edge XANES spectra during the discharge process were displayed in Figure 6b. As the decrease of cell potential, the whiteline of the Bi L_{III}-edge spectra decreased gradually with their edge positions concomitantly shifted towards lower energy position. This indicates that Bi ions are mainly responsible for the charge transfer during the electrochemical cycling process. As observed in Figure 3c, the Bi³⁺ is reduced to Bi⁰ via three-step, three electron reduction process.

The theoretical capacity of BiFeO₃, if calculated according to the formula of $\frac{NF}{M}$, where N is the number of electrons transferred, F is the Faraday constant and M is the molecular weight of the active material, would be about 257 mAh/g (3 electrons transfer). Further insertion of Li⁺ ions via Li₂Bi formation contributes another 2-electron transfer, and make the total 1st cycle discharge capacity of 428.3 mAh/g. This is less than half of what was observed in Figure 3a. (~1000 mAh/g) Similar large capacity has also been observed in CoO[27] and CoS[28], where a transition from Co²⁺ to Co nanoparticles embedded in the Li₂O matrix was proposed as the lithium storage mechanism. In addition, the polymer layers grown in the surface of the electrodes may also play a very important role in this capacity enhancement. In the BiFeO₃ case, oxygen anions may also help to balance the charge, which contribute to the large discharge capacity.

4. SUMMARY

Powdered BiFeO₃ was synthesized using a molten salt method and was investigated as electrode material for lithium battery applications. The 1st discharge capacity of BiFeO₃ vs Li battery is ~ 1000 mAh/g, if one uses a cutoff voltage of 0.05 V. During the discharge process, BiFeO₃ diffraction peaks shifts to lower angle position, due to the insertion of lithium ions into the electrode matrix. Lithiated BiFeO₃ has larger resistance compared with the pristine BiFeO₃ and contributes to large polarization during the subsequent electrochemical cycling process. At the end of the discharge process, LiBi alloy formation was observed, with the main phase in the form of Li₂Bi. Li₂Bi alloy is not fully reversible towards lithium intercalation/extraction and decomposes to metallic Bi. No diffraction peaks of Fe and Bi are observed during the 1st discharge process. Fe K-edge XANES spectra of the fully discharged product is similar to that of the pristine material and indicates that Fe ions are not reduced in the discharge process. During the discharge process, the whiteness of the Bi L_{III}-edge XANES spectra gradually decreased and the Bi L_{III}-edge concomitantly shifts towards lower energy position. This indicates that Bi ions are mainly responsible for the charge balance during the Li insertion process. The reduction of Bi as the gradual insertion of Li ions, is a three step reduction process. Future work to stabilize the lithiated BiFeO₃ lattice is ongoing.

5. ACKNOWLEDGEMENTS

Wen Wen thanks the Institutional Innovation grant (Grant Number: O95501E061) of the Shanghai Institute of Applied Physics, CAS for the financial support. Zhou Xingtai thanks the Ministry of Science and Technology for the national key fundamental research program financial support (Grant Number: 2010CB934500) and the Science and Technology Commission of Shanghai Municipality for the financial support (Grant Number: 1052nm07800). The authors also thank beamlines BL14B1 and BL14W1 of SSRF (Shanghai Synchrotron Radiation Facility) for providing the beam time.

REFERENCES

- [1] M.K. Aydinol, A.F. Kohan, G. Ceder, K. Cho, and J. Joannopoulos, *Phys. Rev. B* 56, 1354 (1997).
- [2] Y.W. Tsai, B.J. Hwang, G. Ceder, H.S. Sheu, D.G. Liu, and J.F. Lee, *Chem. Mater.*, 17, 3191 (2005).
- [3] Y. Shin, and A. Manthiram, *Electrochim. Acta*, 48, 3583 (2003).
- [4] J.W. Stevenson, T.R. Armstrong, R.D. Carneim, L.R. Pederson, and W.J. Weber, *J. Electrochem. Soc.*, 143, 2722 (1996).
- [5] P. Lacorre, F. Goutenoire, O. Bohnke, R. Retoux, and Y. Lali-gant, *Nature*, 404, 856 (2000).
- [6] D.D. Fontaine, G. Ceder, and M. Asta, *Nature*, 343, 544 (1990).
- [7] J. Li, H.M. Dahn, R.J. Sanderson, A.D.W. Todd, and J.R. Dahn, *J. Electrochem. Soc.*, 155, A975 (2008).
- [8] Y. Sharma, N. Sharma, G.V.S. Rao, and B.V.R. Chowdari, *Chem. Mater.*, 20, 6829 (2008).
- [9] K. Imaki, M. Nakayama, Y. Uchimoto, and M. Wakihara, *Solid State Ionics*, 172, 73 (2004).
- [10] M. Nakayama, K. Imaki, H. Ikuta, Y. Uchimoto, and M. Wakihara, *J. Phys. Chem. B*, 106, 6437 (2002).
- [11] Y.J. Shan, L.Q. Chen, Y. Inaguma, M. Itoh, and T. Nakamura, *J. Power Sources*, 54, 397 (1995).
- [12] D.W. Zhang, S. Xie, and C.H. Chen, *J. Electroceramics*, 15, 109 (2005).
- [13] H. Xia, F. Yan, M.O. Lai, L. Lu, and W.D. Song, *Funct. Mater. Lett.*, 2, 163 (2009).
- [14] J. Chen, X.R. Xing, A. Watson, W. Wang, R.B. Yu, J.X. Deng, L. Yan, C. Sun, and X.B. Chen, *Chem. Mater.*, 19, 3598 (2007).
- [15] B.H. Toby, *J. Appl. Crystallogr.*, 38, 1040 (2005).
- [16] B. Ravel, and M. Newville, *J. Synchrotron Rad.*, 12, 537 (2005).
- [17] W. Wen, B. Kumarasamy, S. Mukerjee, M. Auinat, and Y. Ein-Eli, *J. Electrochem. Soc.*, 9, A1902 (2005).
- [18] S. Ghosh, W. Wen, C.R. Urian, C. Heath, V. Srinivasamurthi, W.M. Reiff, S. Mukerjee, V. Naschitz, and S. Licht, *Electrochem. Solid-State Lett.*, 6, A260 (2003).
- [19] Y. Ein-Eli, S.H. Lu, M.A. Rzeznik, S. Mukerjee, X.Q. Yang, and J. Mcbreen, *J. Electrochem. Soc.*, 145, 3383 (1998).
- [20] JCPDS card 20-169.
- [21] X.T. Gao, S.R. Bare, B.M. Weckhuysen, and I.E. Wachs, *J. Phys. Chem. B*, 102, 10842 (1998).
- [22] G. Wirnsberger, K. Gatterer, H.P. Fritzer, W. Grogger, B. Pillep, P. Behrens, M.F. Hansen, and C.B. Koch, *Chem. Mater.* 13, 1453 (2001).
- [23] JCPDS card 27-422.
- [24] JCPDS card 45-956.
- [25] JCPDS card 27-427.
- [26] JCPDS card 44-1246.
- [27] S. Grugeon, S. Laruelle, L. Dupont, and J.-M. Tarascon, *Solid State Sciences*, 5, 895 (2003).
- [28] P. Poizot, S. Laruelle, S. Grugeon, L. Dupont, and J.-M. Tarascon, *Nature*, 407, 496 (2000).